4-1-2010

Charge diffusion in the field-free region of charge-coupled devices

Ralf Widenhorn
Portland State University

Alexander Weber-Bargioni

Morley M. Blouke
Portland State University

Albert J. Bae

Erik Bodegom
Portland State University

Citation Details
Ralf Widenhorn, Alexander Weber-Bargioni, Morley M. Blouke, Albert J. Bae and Erik Bodegom, (2010) "Charge diffusion in the field-free region of charge-coupled devices", Opt. Eng. 49, 044401.

Optical Engineering 49(4), 044401 (April 2010)

Charge diffusion in the field-free region of charge-coupled devices

Ralf Widenhorn
Alexander Weber-Bargioni[*]
Morley M. Blouke, FELLOW SPIE
Albert J. Bae[†]
Erik Bodegom, MEMBER SPIE
Portland State University
Department of Physics
1719 South West 10th Avenue
Suite 128
Portland, Oregon 97207-0751
E-mail: ralfw@pdx.edu

Abstract. The potential well in back-illuminated charge-coupled devices (CCDs) does not reach all the way to the back surface. Hence, light that is absorbed in the field-free region generates electrons that can diffuse into neighboring pixels and thus decreases the spatial resolution of the sensor. We present data for the charge diffusion from a near point source by measuring the response of a back-illuminated CCD to light emitted from a submicron diameter glass fiber tip. The diffusion of electrons into neighboring pixels is analyzed for different wavelengths of light ranging from 430 to 780 nm. To find out how the charge spreading into other pixels depends on the location of the light spot; the fiber tip could be moved with a piezoelectric translation stage. The experimental data are compared to Monte Carlo simulations and an analytical model of electron diffusion in the field-free region. The presented analysis can be used to predict the charge diffusion in other back-illuminated sensors, and the experiment is universally applicable to measure any type of sensors.
[DOI: 10.1117/1.3386514]

Subject terms: charge-coupled devices; charge-coupled device imagers; point spread functions; modulation transfer functions; absoption; diffusion.

Paper 091033PR received Dec. 30, 2009; revised manuscript received Feb. 12, 2010; accepted for publication Feb. 24, 2010; published online Apr. 23, 2010.

1 Introduction

The spatial resolution of a camera depends on the performance characteristics of its optics and its sensor. Although always limited by the pixel dimensions and fill factor, the diffusion of signal charge can have a profound effect on the sensor's resolution. In both front- and back-illuminated devices, the diffusion of charges in the field-free region degrades the spatial resolution. In front-illuminated CCDs, light that penetrates through the depleted region (absorption length at 780 nm is $\sim 9\ \mu$m) can diffuse freely. Most back-illuminated CCDs are not fully depleted; even for thinned devices, the depletion edge does not reach the back surface. The field-free region can be minimized by additional thinning or by using higher resistivity silicon.[1] However, additional thinning will result in a loss of red and IR response. On the other hand, high-resistivity silicon is more expensive and often of lower quality. Carriers generated near the back surface (absorption length at 430 nm is $<0.4\ \mu$m) diffuse freely through the field-free region before they are collected.

To measure the diffusion of carriers from one pixel into the neighboring pixels, charges have to be generated in a defined region. Diffusion has been measured with a knife edge,[2] a focused light beam,[3,4] or a pinhole mask.[5] We demonstrate a novel method of measuring the charge diffusion in a CCD. A glass fiber tip, similar to that utilized in scanning near-field optical microscopes (SNOM), was used to generate a small light spot. Similar to a SNOM, we were able to move the light spot over the pixel and generate charges with different wavelengths to measure the diffusion, depending on the location of generation and the wavelength. The presented experimental setup is inexpensive and could be used to measure the diffusion of any type of sensor.

Theoretically, the diffusion can be modeled by simulating the random walk of the carrier in the field-free region.[6,7] In order to get an analytical solution, one needs to solve the diffusion or continuity equation.[8–10] A solution to the diffusion equation is available for a point source of electrons at the back surface of the CCD.[5] This solution describes a system where all light is absorbed on the back surface. Although this is a good approximation for blue light, for longer wavelengths the absorption length of the light has to be considered. We will derive a solution that can be applied to different wavelengths of light. This is of major importance because, in most cases, sensors are used over a wide range of wavelengths. A Monte Carlo simulation and the analytical solution yield almost identical results. By comparing the calculated diffusion for different field-free regions to the experimental data, the size of the field-free region is obtained.

2 Experiment

2.1 *Experimental Setup*

The fiber tips were obtained by etching the glass fiber in hydrofluoric acid.[11] After coating them with a palladium metal film, the far end of the tip was cut with a focused ion beam machine. We obtained aperture sizes between 0.5 and

[*]Current address: Lawrence Berkeley National Laboratories, 1 Cyclotron Rd. Berkeley, CA 94720.
[†]Current address: Cornell University, 109 Clark Hall, Ithaca, NY 14853.
0091-3286/2010/$25.00 © 2010 SPIE

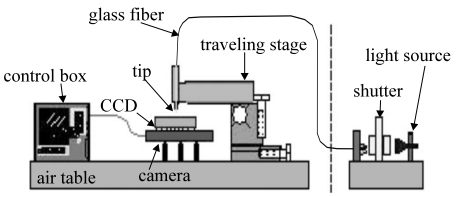

Fig. 1 Schematic of the experimental setup.

1 μm. The tip was mounted on a three-dimensional traveling stage. With micrometer screws, the tip could be placed over the region to be investigated. The scan itself was done with a three-dimensional piezoelectric element, which was integrated in the traveling stage (see Fig. 1). To measure the distance traveled, a precision-measuring tool from Mitutoyo was used for all three dimensions. We used LEDs (peak wavelengths: 430, 565, 650 nm) and a laser diode (peak wavelength: 780 nm) as light sources. Between the fiber end and the light source, a shutter was mounted that was triggered by the camera control box. The chip was a three-phase, n-buried channel, three-level polysilicon back-thinned device (SI032, 12.3×12.3 mm, 512×512 pixels, manufactured by SITe Inc., Tigard, Oregon) with an individual pixel size of 24×24 μm. The CCD was thinned to a thickness of 15 μm.

At the beginning of each scan, the tip was lowered toward the chip until it made contact. Then the tip was raised one-half to 1 μm to achieve measuring distance. The spot size depends on the diameter of the tip aperture and the distance between tip and CCD surface. However, both the theoretical models and the experimental results showed that a small change in the distance and tip size did not a have a large impact on the observed diffusion. By simulating the diffusion of the carriers in the chip, it turned out that, with a pixel size of 24 μm, a spot size of 0.5 μm or a spot size of up to 3 μm changed the resulting diffusion curves only slightly. Hence, scanning the imager with a spot size up to three to five times as large as the fiber tip provides a good agreement between simulation, model, and experiment. Experimentally, the effect of the tip size was verified by comparing two tips of different aperture sizes (500 and 900 nm). The curves obtained with these two different fiber tips were practically identical. Also, we measure the response for distances of a quarter to 7 μm and found that the response as a function of distance changed only for distances of >1 μm.[12] It is also important to note that the larger index of refraction of silicon will decrease the widening of the spot as the light propagates into the pixel. Thus, although the wavelength-dependent diffraction effects makes it difficult to know the exact intensity distribution of the light, the dimensions of the pixels are too large to have an effect on the results in this study.

A sequence off ten pictures taken at the same position with an interval of 10 s between exposures was taken to verify the reproducibility of the data. We found that the amount of charge collected in the center pixel varied by $<0.5\%$. Therefore, we decided to take three images per position as we scanned in micrometer steps over the investigated pixels. The final image was obtained by taking the average of the three exposures and subtracting the dark current. The dark current was obtained by analyzing the dark count of pixels away from the illuminated area. We obtained three dark frames before and after each scan. Using these calibration frames, the dark current of the illuminated pixels can calculated from the dark current of the nonilluminated pixels. This method gives the best estimation of the actual dark count because it reflects the condition of the chip.[13] We also found by scanning different pixels that the choice of the location on the chip did not have an effect on the result.

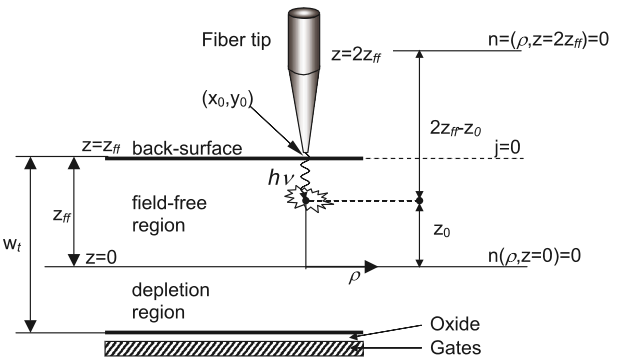

Fig. 2 Schematic of the analytical model.

2.2 *Analytical Model*

Several models for charge diffusion in the field-free region of both back- and front-illuminated CCDs have been developed. These models are generally based on either a Monte Carlo simulation of the random walk of an electron or the solution of the continuity equation. Hopkinson[14] noted that the solution to the continuity equation for a point source of carriers is equivalent to the problem of a charge between two grounded planes. For the case of a point source at the back surface of a back-illuminated CCD, Groom et al.[5] give a solution to the diffusion equation. This solution is applicable for large field-free regions and light that is absorbed close to the back surface. For thinned CCDs, where the field-free region is on the order of 10 μm or less, the penetration depth of incoming light has to be considered. In the following derivation, we generalize the solution to the continuity equation for a point source to all wavelengths.

The generating function of a point source is given by (see also Fig. 2)

$$G = \delta(x-x_0)\,\delta(y-y_0)\,\delta(z-z_0)n(z_0), \tag{1}$$

where (x_0, y_0) are the coordinates of the light spot illuminating the surface of the chip. The y-axis is along the channel stop, and the x-axis is perpendicular to it. The charges n (in our case electrons) are generated at z_0. The penetration depth, or in other words, the wavelength of the incoming light, determines the probability that a carrier is generated at a certain z_0. The steady-state diffusion equation for the free electron concentration, n, in the field-free region with G as in Eq. (1) is given by

$$D_n\nabla^2 n + \delta(x-x_0)\,\delta(y-y_0)\,\delta(z-z_0)n(z_0) = 0, \tag{2}$$

where D_n is the diffusion constant for electrons. The free electron concentration must satisfy the boundary condition that it is zero at the depletion edge,

$$n(\rho, z=0)=0, \tag{3}$$

where $\rho=\sqrt{(x-x_0)^2+(y-y_0)^2}$ is the radial distance from (x_0, y_0).

It is assumed that the back side of the CCD is treated such that a potential barrier is generated. Therefore, we assume the back surface of the CCD is reflective to negative charges. Electrons reflected from the back surface ($z=z_{ff}$) of the CCD have to diffuse another z_{ff} before they reach the depletion edge. Instead of assuming the back surface reflecting and measuring the reflected carriers at the depletion edge, one can remove the back surface and determine the diffusion current at an imaginary plane at $z=2z_{ff}$. This results in the boundary condition

$$n(\rho, z=2z_{ff})=0. \tag{4}$$

For any given z_0, the problem as stated in [Eq. (2)–(4)] is equivalent to a system of a point charge between two grounded plates $2z_{ff}$ from each other. Jackson gives the resulting charge distribution on the upper plate.[15] There, the charge distribution on the plate is proportional to the electric field, which is given by the gradient of the potential at the plate. We are interested in the probability density current, which can be defined as

$$j=-D_n \nabla n. \tag{5}$$

The probability density current for the reflected carriers should be distributed exactly in the same way as the charge density on the upper plate in Jackson

$$j_r(\rho)=\frac{n(z_0)}{2\pi}\int_0^\infty \frac{\sinh(kz_0)}{\sinh(2kz_{ff})}kJ_0(k\rho)dk. \tag{6}$$

The nonreflected probability density current follows from symmetry considerations as:

$$j_{nr}(\rho)=\frac{n(z_0)}{2\pi}\int_0^\infty \frac{\sinh[k(2z_{ff}-z_0)]}{\sinh(2kz_{ff})}kJ_0(k\rho)dk, \tag{7}$$

where J_0 is the zero order Bessel function of the first kind. These integrals (see, for example, Gradshteyn and Ryzhik[16]) can be solved and lead to

$$j_r(\rho)=\frac{n(z_0)}{4z_{ff}^2}\sum_{i=1}^{\infty}(-1)^i i \sin\left(\frac{i\pi z_0}{2z_{ff}}\right)K_0\left(\frac{i\pi\rho}{2z_{ff}}\right), \tag{8}$$

$$j_{nr}(\rho)=\frac{n(z_0)}{4z_{ff}^2}\sum_{i=1}^{\infty}(-1)^i i \sin\left[\frac{i\pi(2z_{ff}-z_0)}{2z_{ff}}\right]K_0\left(\frac{i\pi\rho}{2z_{ff}}\right). \tag{9}$$

K_0 is the zero-order modified Bessel function. Note that z_0 is measured form the depletion edge (see Fig. 2). The charge generation probability depends on the penetration depth λ and can be expressed as follows:

$$n(z_0)=\frac{1}{\lambda}\exp\left(-\frac{z_{ff}-z_0}{\lambda}\right), \tag{10}$$

where $n(z_0)$ is normalized such that

$$\int_{-\infty}^{z_{ff}} n(z_0)dz_0=1. \tag{11}$$

Recombination can be neglected in our case and for any given generation depth z_0

$$\int_0^\infty 2\pi j_{nr}\rho d\rho+\int_0^\infty 2\pi j_r\rho d\rho=n(z_0). \tag{12}$$

Of course, in reality, the CCD does not extend to infinity. However, the Bessel function approaches zero very rapidly with increasing ρ. Therefore, for realistic z_{ff}, the integral converges to $n(z_0)$ in a few pixels. For a given photon flux, the fraction absorbed in the field-free region is given by

$$\int_0^{z_{ff}} n(z_0)dz_0=1-\exp\left(-\frac{z_{ff}}{\lambda}\right). \tag{13}$$

Especially for radiation in the red or near IR, the finite thickness of the CCD must be considered. The fraction of photons absorbed in the depletion region is given by

$$\int_{z_{ff}-w_t}^0 n(z_0)dz_0=\exp\left(-\frac{z_{ff}}{\lambda}\right)-\exp\left(-\frac{w_t}{\lambda}\right), \tag{14}$$

where w_t is the thickness of the CCD chip. Neglecting the internal reflection of light in the CCD, the fraction of photons detected by the CCD can be calculated as

$$\int_{z_{ff}-w_t}^{z_{ff}} n(z_0)dz_0=1-\exp\left(-\frac{w_t}{\lambda}\right). \tag{15}$$

The fraction of electrons counted in a rectangular region defined by the opposite points (x_l, y_u) and (x_r, y_d), is given by

$$j_{\text{diff}}=\frac{\int_{x_l}^{x_r}\int_{y_l}^{y_u}\int_0^{z_{ff}}\exp(-z_{ff}-z_0/\lambda)(j_{nr}+j_r)dxdydz_0}{\lambda(1-\exp(-w_t/\lambda))}. \tag{16}$$

If the light spot falls on the rectangle, then one has to add the carriers absorbed in the depletion region

$$j_{\text{abs}}=\frac{\exp[-(z_{ff}/\lambda)]-\exp[-(w_t/\lambda)]}{\lambda[1-\exp(-w_t/\lambda)]}. \tag{17}$$

Note that if none of the carriers diffuse into neighboring pixels, the sum of j_{diff} and j_{abs} as given by Eqs. (16) and (17) is equal to unity.

3 Results

3.1 *Experimental Results*

We present the data obtained from a scan with a 0.7-μm fiber tip approximately parallel to the channel stops. The piezoelement's traveling range of 30 μm is slightly larger than the size of a pixel. Each data set is a scan over the center of one pixel. The center of the pixel was found by placing the tip such that the signals above and below the main pixel were identical and the signals to the right and left of the main pixel were identical. When collecting data, we observed that for some scans there was a drift of up to

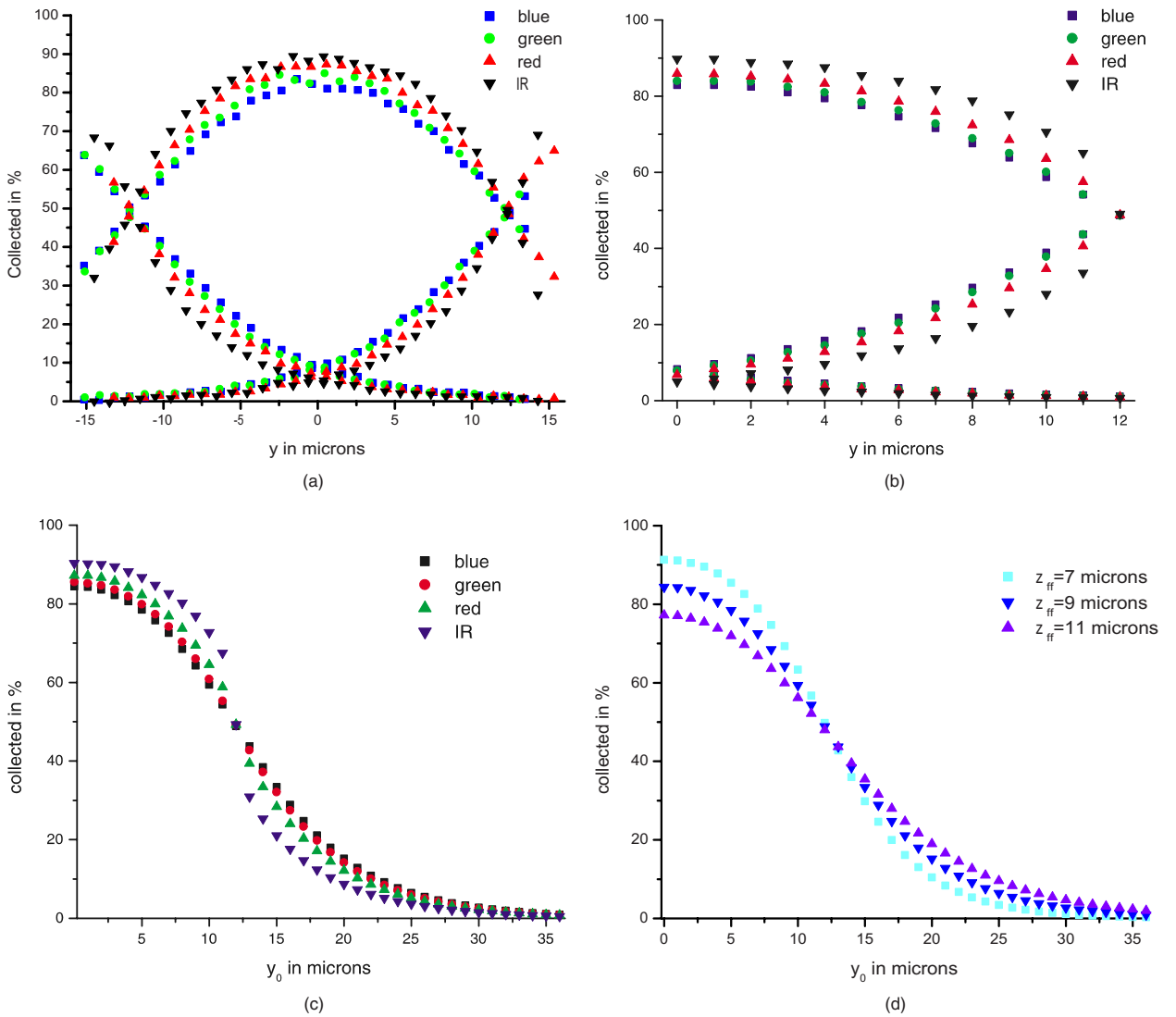

Fig. 3 Data for the diffusion of electrons in the field-free region. (a) experimental data for scans over one pixel. The value for three rows are depicted for four different wavelengths, (b) simulated diffusion for scans over half a pixel for four wavelengths with an assumed field-free region of *zff*=9 μm, three rows are displayed, (c) analytical model of the diffusion for four wavelength and *zff*=9 μm, the main row is displayed for a scan over one and a half pixels, and (d) analytical model for blue light and three different *zff*s.

1 μm perpendicular to the intended scan direction. Therefore, in the data analysis, we summed over the pixels that were in the same row. Figure 3(a) shows the data for scans of four wavelengths. For each wavelength, the values for three different rows are shown. When the fiber tip is placed in the middle of the main pixel (y=0 μm) the percentage absorbed in the main row is approximately given by blue light=83.5%, green light=85%, red light=87.5%, and infrared light=89.5%. At y=0 μm, the value for the row above and below are equal. As one would expect, the peak value increases with increasing wavelength. At y=12 μm, the tip is between two pixels and the value for the main row is approximately equal to the row below it. As we scan upward, the value for this row decreases. At y=−12 μm, the tip is located between the main row and the row above it. Summing the values of the three rows, one finds that almost 100% of the electrons are collected in these three rows. Hence, for all wavelengths, the diffusion further than a complete pixel length is very small.

3.2 *Monte Carlo Simulation*

The random walk was simulated in a similar way as described previously.[7] For any given position and wavelength of the point light source, carriers were generated randomly in a 1-μm radius. The exact intensity distribution and spot size of the light spot in the actual experiment was not measured. Fraunhofer diffraction, as an upper limit for the radius, suggests that 1 μm is a good estimate of the actual experiment. Although it would be desirable to experimentally measure the intensity distribution of the light spot on the surface of the CCD, it is important to note that the simulation is not very sensitive to small changes in the size

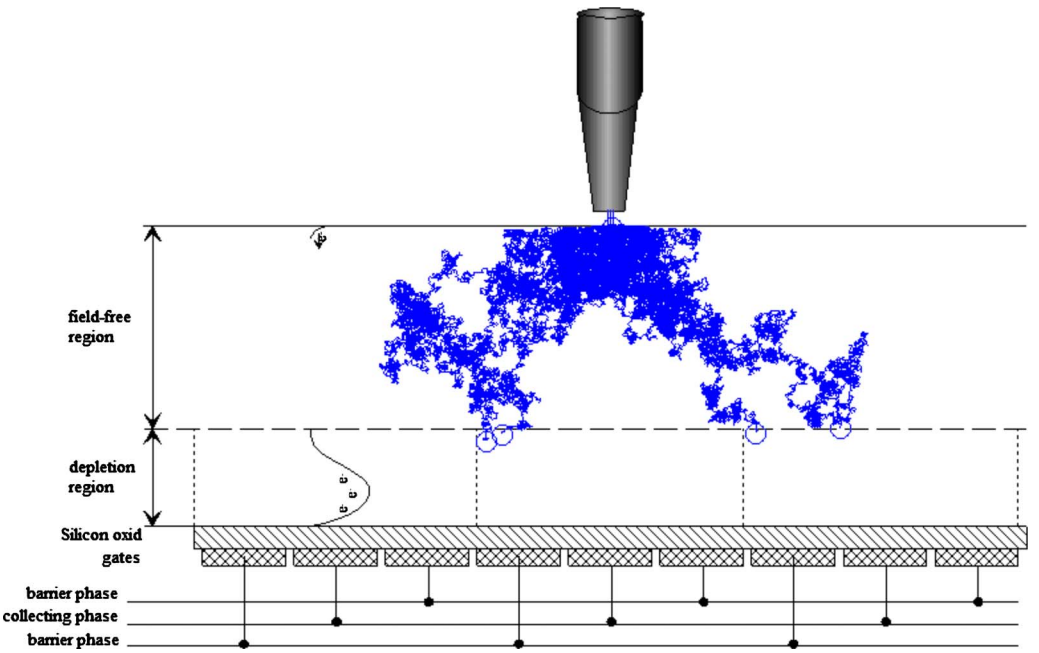

Fig. 4 Schematic of the random walk for four electrons generated by blue light.

of the spot. We do not consider optical cross-talk and assume that the light spot does not further widen in the CCD. This approximation can be justified by recalling that silicon has a large index of refraction. The photons in the light spot are absorbed randomly with a probability dependent on the penetration depth at a given wavelength.

We used the following absorption lengths: $\lambda = 0.385\ \mu$m at 430 nm, $\lambda = 1.724\ \mu$m at 565 nm, $\lambda = 3.33\ \mu$m at 650 nm, and $\lambda = 9.09\ \mu$m at 780 nm. After generation, each electron begins its random walk through the field-free region. The path length for each random step in the data presented here was 1 μm. This is significantly larger than the mean free path of an electron. We also conducted simulations with a path length of 100 nm. We found, in agreement with Janesick et al.,[7] that the results are independent of the assumed path length. It is important to note that simulations with a very short path length are very time intensive. In our simulation, the light spot was placed in 1-μm steps from the middle of the pixel ($y = 0\ \mu$m) to the boundary of the pixel ($y = 12\ \mu$m). At each point, the random walks of 10,000 electrons were followed to the depletion edge. At this location, the electron was considered as collected by the potential of the corresponding pixel. Figure 4 shows the random walk of four electrons until they are collected by the potential well. As indicated by the small circles, two of the electrons diffused into a neighboring pixel. The charge distribution resulting from the random walk of 10,000 electrons was weighted, and the carriers absorbed in the depletion region were added (the weighting was done as discussed in Section 3). At $y = 12\ \mu$m, only half the carriers absorbed in the depletion region are counted as absorbed in the main row. Figure 3(b) shows the graphs for the same three pixel rows as in the experimental part for a assumed field-free region of 9 μm. The plot depicts the same region as the right half of Fig. 3(a). The collected percentage is the sum of pixels in the same row. As expected, the diffusion depends on the wavelength. A more detailed comparison between the experimental data and the simulation follows.

3.3 *Analytical Model*

To analyze the data from a scan parallel to the channel stops, the integral in Eq. (16) has to be solved for different y_0. We integrated Eq. (16) numerically with the Monte Carlo method. To account for the finite spot size at a given position, y_0 is substituted by $y_0 \pm rnd * r$, where rnd are random numbers between 0 and 1, and $r = 1\ \mu$m is the radius of the light spot. Without loss of generality, x_0 can be set to 0. The integration boundaries as given by the pixels size are $y_d = -12\ \mu$m and $y_u = 12\ \mu$m. The Bessel function converges rapidly to 0 for large ρ. Therefore, integration over 5 pixels ($x_l = -60\ \mu$m and $x_r = 60\ \mu$m) is sufficient. Note that our experimental data support the assumption that the carrier diffusion over more than 2 pixels can be neglected. Figure 3(c) shows the percentage collected in the main row for a scan from $y_0 = 0-36\ \mu$m for $z_{ff} = 9\ \mu$m. The effect of absorption in the depletion region can be seen best for infrared light. Close to the pixel boundary ($y_0 = 12\ \mu$m), the collected percentage falls off rapidly.

At $y_0 = 11\ \mu$m, all electrons generated in the depletion region count toward the collected percentage. If the light spot is located between two pixels ($y_0 = 12\ \mu$m), then only half the electrons absorbed in the depletion region fall in the collecting region. Electrons generated in the depletion region at $y_0 = 13\ \mu$m are not collected in the region of interest. The influence of the size of the field-free region, can be seen in Fig. 3(d). Depicted is the collected fraction in the main row for $z_{ff} = 7\ \mu$m, $z_{ff} = 9\ \mu$m, and $z_{ff} = 11\ \mu$m.

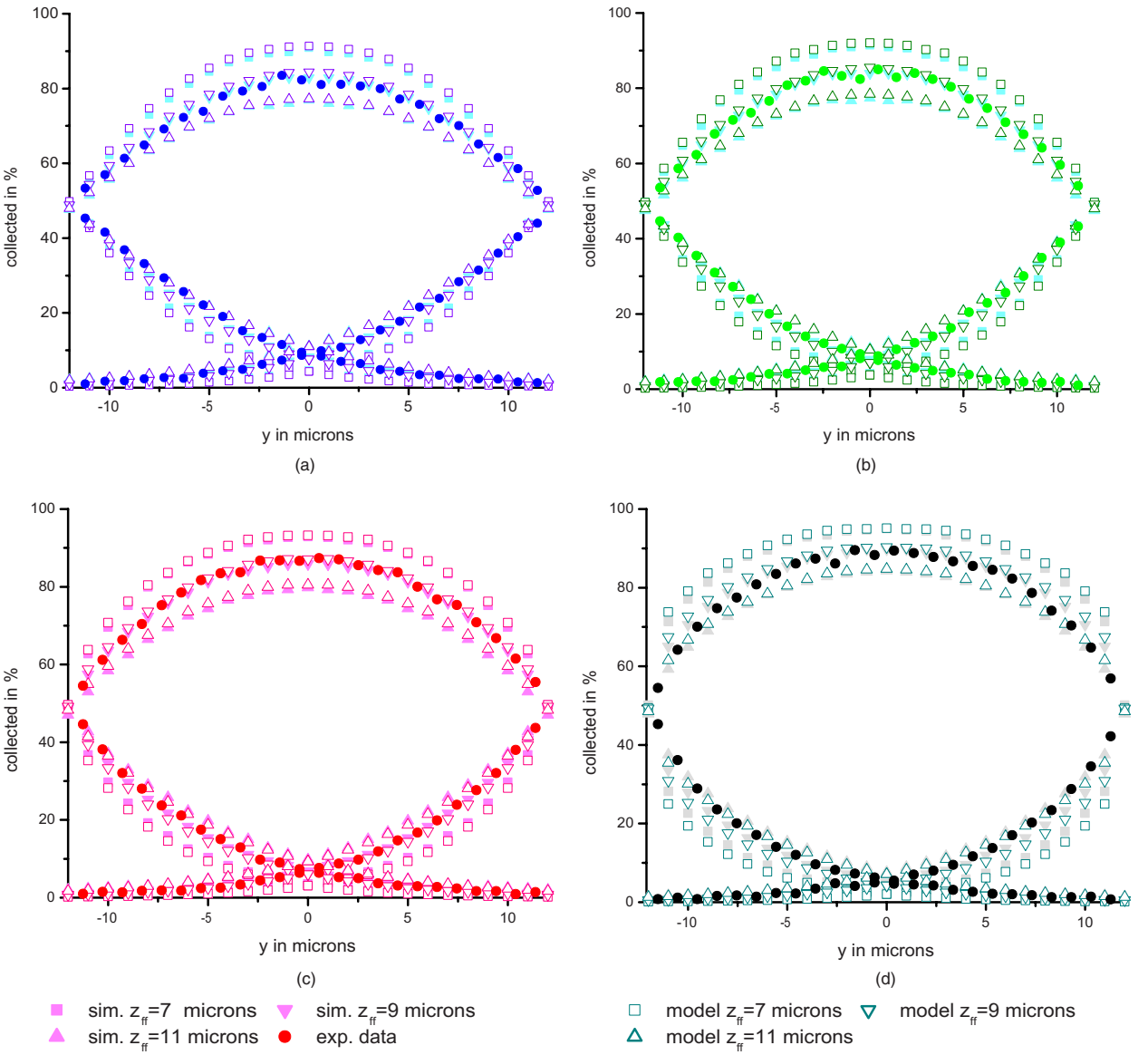

Fig. 5 Comparison of the experimental data, simulation, and analytical model. The solid circle represent the experiment results. The other solid symbols correspond to the simulation, and the open symbols correspond to the data from the analytical model. For the same field-free region, the simulated data and the data from the model are very close and overlap: (a) blue light 430 nm, (b) green light 565 nm, (c) red light 650 nm, and (d) infrared light 780 nm.

4 Discussion

In order to find the size of the field-free region and to see whether the simulation and the analytical model agree with each other, one needs to compare the plots for different wavelengths and field-free regions. The simulation was done from $y=0$ to 12 μm. However, the collected fraction is a function of the absolute value of y. Hence, using the data for positive y, Fig. 3(b) can be extended to $y=-12$ μm. The scan of the analytical model [Fig. 3(c)] can be separated into three parts. From $y_0=0$ to 12 μm, the graph can be compared to the main row of the experimental data and the simulation. The section from $y_0=12$ to 36 μm corresponds to a scan from $y_0=-12$ to 12 μm for the row below the main row. The model is also symmetrical about $y_0=0$. Therefore, a graph similar to Fig. 3(a) can be generated based on the data of a scan from $y_0=0$ to 36 μm. Figure 5 displays the curves of the simulation and the model for three different field-free regions and the experimental data. The first important finding is that simulation and analytical model are in agreement with each other for all λ and z_{ff}. Hence, for the problem described here, one does not need a simulation and the analytical model can be used. The second important result is that, for all wavelengths, the experiment can be modeled with a field-free region of 9 μm. It is also interesting that for blue, green, and red light, the models agree with the experimental data for all positions of the fiber tip. At 780 nm, the 9 μm curves fit the experimental data very well for $|y|<5$ μm. When the tip is placed close to the boundary between pixels, there is a slight difference with

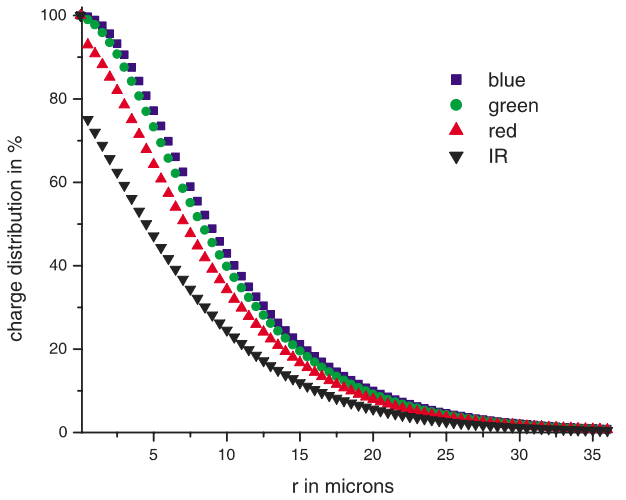

Fig. 6 Marginal distribution for a perfect point source at the center of a pixel. The data points represent the charge fraction outside a circle of radius r for zff=9 μm.

the model. This is most likely due to a widening of the beam in the CCD or the fact that we did not account for the effect of the channel stops.

For manufacturers, it is important to know how the spatial resolution of the CCD changes with pixel size, wafer thickness, and field-free region. The experiment and calculations show that, in principle, a single measurement at the center of one pixel gives a good indication of the spatial resolution and the field-free region. We expect that the analytical model is generally applicable for all back-side CCDs, where the influence of the channel stops can be neglected. For an astronomer, it is interesting to know how well a CCD depicts a point light source. Figure 6 shows the electron diffusion distribution as a function of the distance from the origin for a perfect point light source based on the model described above. In the ideal case, the distribution would be a δ function. Because the absorption length of light in silicon is wavelength dependent, the distribution differs significantly for different colors of light. For example, if one wants 75% of the electrons within a radius r, then one needs a circle of $r \geq 13.7$ μm at 430 nm and a circle of $r \geq 10$ μm at 780 nm. There are two reasons why the distributions depend on the wavelength: First, at 780 nm, photons absorbed in the field-free region, generate more electrons close to the depletion edge. Second, unlike for blue and green light, for infrared light a large fraction of photons is absorbed in the depletion region.

5 Conclusion

We solved the diffusion equation for free electrons in the field-free region of a back-illuminated CCD for a wavelength-dependent generating function. The solution is validated for different wavelengths of light by comparison to a standard Monte Carlo simulation. We developed a novel and inexpensive setup, similar to an SNOM, to measure the spreading of electrons generated by a subpixel light spot. The setup is not limited to back-illuminated CCD sensors but can also be used for example for CMOS imagers. By comparison between experimental data and analytical model, the field-free region of the CCD used was calculated to be ~9 μm. Knowing the size of the field-free region, the model can be used to predict how the spatial resolution changes with wavelength, pixel size, field-free region, or wafer thickness.

Acknowledgments

This research was supported by a Grant-in-Aid of Research from the National Academy of Sciences, administered by Sigma Xi, the Scientific Research Society and by the Tektronix Corporation.

References

1. D. E. Groom, "Recent progress on CCDs for astronomical imaging," *Proc. SPIE* **4008**, 634–645 (2000).
2. S. E. Reichenbach, S. K. Park, and R. Narayanswamy, "Characterizing digital aquisition devices," *Opt. Eng.* **30**(2), 170–177 (1991).
3. D. Kavaldjiev and Z. Ninkov, "Experimental measurement of the variation in sensitivity within a single pixel of a CCD," *Proc. SPIE* **3019**, 42–49 (1997).
4. A. Piterman and Z. Ninkov, "Measurements of the subpixel sensitivity for a backside-illuminated CCD," *Proc. SPIE* **3965**, 289–297 (2000).
5. D. E. Groom, P. H. Eberhard, S. E. Holland, M. E. Levi, N. P. Palaio, S. Perlmutter, R. J. Stover, and M. Wei, *Point-Spread Function in Depleted and Partially Depleted CCDs*, Astrophysics and Space Science Library 2000, vol. **252**, pp. 201–206, Kluwer Academic Publishers, Dordrecht (1999).
6. J. P. Lavine, W.-C. Chang, C. N. Anagnostopoulos, B. C. Burkey, and E. T. Nelson, "Monte Carlo simulation of the photoelectron crosstalk in silicon imaging devices," *IEEE Trans. Electron Devices* **32**, 2087 (1985).
7. J. Janesick T. Elliott, G. Garmire, "CCD advances for x-ray measurements," *Proc. SPIE* **597**, 364–380 (1985).
8. M. H. Crowell and E. F. Labuda, "The silicon diode array camera tube," *Bell Syst. Tech. J.* **48**, 1481 (1969).
9. M. M. Blouke and D. A. Robinson, "A method for improving the spatial resolution of frontside-illuminated CCD's," *IEEE Trans. Electron Devices* **28**(3), 251 (1981).
10. E. G. Stevens and J. P. Lavine, "An analytical, aperture, and two-layer carrier diffusion MTF and quantum efficiency model for solid-state image sensors," *IEEE Trans. Electron Devices* **41**(10), 1753 (1994).
11. R. Stöckle, C. Fokas, V. Deckert, R. Zenobi, B. Sick, B. Hecht, and U. P. Wild, "High-quality near-field optical probes by tube etching," *Appl. Phys. Lett.* **75**, 160 (1999).
12. A. Weber, "Field-free regions in charge-coupled devices," Master's Thesis, Portland State University (2002).
13. R. Widenhorn, A. Rest, M. M. Blouke, R. L. Berry, and E. Bodegom, "Computation of dark frames in digital imagers," *Proc. SPIE* **6501**, 650103 (2007).
14. G. R. Hopkinson, "Charge diffusion effects in CCD x-ray detectors: I. Theory," *Nucl. Instrum. Methods Phys. Res.* **216**, 423 (1983).
15. J. D. Jackson, *Classical Electrodynamics*, 2nd ed., Wiley, Hoboken, NJ, p. 133 (1975).
16. I. S. Gradshteyn and I. M. Ryzhik, *Table of Integrals, Series, and Products* (trans. A. Jeffrey), Academic Press, New York (1965).

Biographies and photographs of the authors not available.